

Unusual Formation of ZnCo_2O_4 3D Hierarchical Twin Microspheres as a High-Rate and Ultralong-Life Lithium-Ion Battery Anode Material

Jing Bai, Xiaogang Li, Guangzeng Liu, Yitai Qian, and Shenglin Xiong*

A facile two-step strategy involving a polyol method and subsequent thermal annealing treatment is successfully developed for the large-scale preparation of ZnCo_2O_4 various hierarchical micro/nanostructures (twin microspheres and microcubes) without surfactant assistance. To the best of our knowledge, this is the first report on the synthesis of ZnCo_2O_4 mesoporous twin microspheres and microcubes. More significantly, based on the effect of the reaction time on the morphology evolution of the precursor, a brand-new crystal growth mechanism, multistep splitting then in situ dissolution recrystallization accompanied by morphology and phase change, is first proposed to understand the formation of the 3D twin microspheres, providing new research opportunity for investigating the formation of novel micro/nanostructures. When evaluated as anode materials for lithium-ion batteries (LIBs), ZnCo_2O_4 hierarchical microstructures exhibit superior capacity retention, excellent cycling stability at the 5 A g^{-1} rate for 2000 cycles. Surprisingly, the ZnCo_2O_4 twin microspheres show an exceptionally high rate capability up to the 10 A g^{-1} rate. It should be noted that such super-high rate performance and cycling stability at such high charge/discharge rates are significantly higher than most work previously reported on ZnCo_2O_4 micro/nanostructures and ZnCo_2O_4 -based heterostructures. The ZnCo_2O_4 3D hierarchical micro/nanostructures demonstrate the great potential as negative electrode materials for high-performance LIBs.

of applications, including mobile devices, electric vehicles (EVs)/hybrid electric vehicles (HEVs) and even energy storage systems (ESSs). To meet the requirements of these applications, further improvements in terms of energy power, densities and cycle time are required. Because of their intrinsic limits in performance, conventional bulk electrode materials are unable to completely fulfill the increasing demands. It has been widely acknowledged that nanosized cathode/anode materials provide higher rate capability by means of decreasing lithium-ion diffusion distances and increasing the contact area between the electrode and the electrolyte.^[1–5] However, electrodes made from nanoscaled materials tend to collapse easily since they cannot be packed as densely on the current collector as micrometer-sized materials. In addition, the low tap density of the nanoscale materials results in a low volumetric energy density. Generally speaking, an optimal structure for electrode materials with both high energy density and high rate

1. Introduction

Nowadays, Lithium-ion batteries (LIBs) are expected to satisfy the rate capability and capacity requirements for a range

capacity should be a porous microstructure composed of primary nanocrystallines tightly compacted to form 3D channels for ion diffusion.^[5–9] Therefore, in order to further improve the performances of LIBs, it is highly desirable to prepare materials with not only involving nanometer-sized subunits for high specific capacity and good rate performance, but also possessing a stable 3D porous hierarchical microstructure with excellent ability for improving the cycling stability.

Spinel transition-metal oxides are a family of important technological materials because they have intriguing properties and wide-spread applications in many fields such as drug delivery, catalysts, energy storage and conversion, and so on.^[10–13] In particular, as a new class of anode electrode materials for LIBs, transition metal oxide (Co_3O_4) can in principle deliver high theoretical capacity of $\sim 890 \text{ mAh g}^{-1}$ and thus has been widely investigated during the past several years.^[1,14–21] However, due to the fact that on the one hand, it usually suffers from poor capacity retention during cycling and/or poor rate capability, on the other hand, cobalt is toxic, expensive and high lithium redox potential (2.2–2.4 V vs. Li^+/Li). Numerous efforts are made towards replacing Co ions of Co_3O_4 partially by eco-friendly and cheaper alternative metal ions. For this

Dr. J. Bai, X. G. Li, Dr. G. Z. Liu,
Prof. Y. T. Qian, Prof. S. L. Xiong
Key Laboratory of the Colloid and
Interface Chemistry (Shandong University)
Ministry of Education
and School of Chemistry and Chemical Engineering
Shandong University
Jinan 250100, PR China
E-mail: chexsl@sdu.edu.cn

Prof. S. L. Xiong
CAS Key Laboratory of Materials for Energy Conversion
Prof. Y. T. Qian
Hefei National Laboratory for Physical Science at Microscale
and Department of Chemistry
University of Science and Technology of China
Hefei, Anhui 230026, PR China
Dr. G. Z. Liu
Department of Chemistry, Qilu Normal University
Jinan, Shandong 250100, PR China



DOI: 10.1002/adfm.201303442

purpose, preliminary anodic materials and corresponding properties have been reported on NiCo_2O_4 ,^[22,23] $\text{CoMn}_2\text{O}_4/\text{MnCo}_2\text{O}_4$,^[5,24,25] and ZnCo_2O_4 .^[26–31] In this study, ZnCo_2O_4 is selected as the research material because it is an attractive candidate for evaluation as anode for LIBs. It should be mentioned that it can store Li^+ through not only the conversion reaction, but also including the alloying-de-alloying reaction between Zn and Li ($\text{Zn} + \text{Li}^+ + \text{e}^- \leftrightarrow \text{LiZn}$), which results in a high theoretical capacity of $\sim 900 \text{ mA h g}^{-1}$.^[26] Various methods have been reported to enhance the cycling stability of ZnCo_2O_4 including the usage of nano/microstructures with better structural stability for accommodating volume changes (nanoparticles,^[26,27] nanowires,^[28] nanotubes,^[29] and microspheres,^[30] and ZnCo_2O_4 -based composites.^[31] However, both cycling performance and rate capabilities of ZnCo_2O_4 anodes that have been reported need more improvement to satisfy the higher and higher demands of electric vehicles with high energy consumption. Therefore, it is of great importance to synthesize high-quality ZnCo_2O_4 electrode materials with excellent electrochemical performance.

Inspired by those previous efforts, in this contribution, we have devised a convenient solution-based method for preparation of a new type of ZnCo_2O_4 hierarchical micro/nanostructures without surfactant assistance. To the best of our knowledge, this is the first report on the preparation of ZnCo_2O_4 mesoporous twin microspheres and microcubes. More significantly, based on the effect investigation of the reaction time on the morphology evolution of the precursor, a novel growth mechanism, multistep-splitting-then-in situ-dissolution-recrystallization accompanied by morphology and phase change, is first proposed to understand the formation of the 3D twin microspheres. The as-synthesized porous hierarchical microstructures (twin spheres and microcubes) possess many structural merits. Specifically, the nanosized primary particles facilitate Li^+ ion transport by decreasing the diffusion distance. Furthermore, the porous structures made of primary particles with uniform distribution permit fine penetration of the electrolyte into the inner active materials. On the other hand, the micrometer size and robust framework of the secondary porous microstructures can effectively buffer the aggregation of particles. As a result, when evaluated as anode materials for LIBs, both ZnCo_2O_4 hierarchical microstructures displayed excellent cycling stability at the 5 A g^{-1} rate for 2000 cycles. Surprisingly, the ZnCo_2O_4 twin microspheres shows an exceptionally high rate capability up to the 10 A g^{-1} rate. These superiorities further confirm the advantages of the porous microstructures consisting of numerous primary nanocrystallites, which will be further discussed in detail below.

2. Result and Discussion

We first synthesized monodisperse $\text{Zn}_{0.33}\text{Co}_{0.67}\text{CO}_3$ twin microspheres with an “8”-shaped structure through a modified polyol process (Supporting Information, SI-1). FESEM images of the as-formed $\text{Zn}_{0.33}\text{Co}_{0.67}\text{CO}_3$ twin microspheres are displayed in Figure S1(a,b), which are at close to 100% morphological yield with average diameter in the range of $2.5\text{--}3.0 \mu\text{m}$. Via the current preparative method, when the amount of ammonium

bicarbonate was increased from 15 to 30 mmol, uniform $\text{Zn}_{0.33}\text{Co}_{0.67}\text{CO}_3$ microcubes rather than twin microspheres were obtained (Figure S1(c,d)). More significantly, based on the observation over the temporal evolution of the $\text{Zn}_{0.33}\text{Co}_{0.67}\text{CO}_3$ twin spheres, a multistep-splitting-in situ-dissolution-recrystallization growth mechanism is proposed to understand the formation of the 3D hierarchical twin nanostructures for the first time, which will be discussed in detail below. Further materials characterization with X-ray diffraction (XRD) and thermogravimetric analysis (TGA) can be found in the Supporting Information (Figure S2 & 3). Mesoporous ZnCo_2O_4 twin microspheres and microcubes were obtained via a topotactic conversion from $\text{Zn}_{0.33}\text{Co}_{0.67}\text{CO}_3$ twin microspheres and microcubes in laboratory air.

In Figure 1a, the panoramic FESEM image reveals that the product is composed of uniform microspheres with diameters of $2.5\text{--}3.0 \mu\text{m}$. It should be noted that the hierarchical microstructures are quite thermally stable without structural collapse (Figure 1). Very interestingly, these twinned spheres still maintain an dumbbell-shaped structure from the high-magnification FESEM images (Figure 1b,c), which completely inherit from the corresponding precursors even after the heat treatment. From a higher-magnification as shown in Figure 1c, it is revealed that ZnCo_2O_4 twin microspheres are highly porous and composed of numerous highly uniform nanosized-sized primary nanoparticles. The use of the pre-grown $\text{Zn}_{0.33}\text{Co}_{0.67}\text{CO}_3$ as the precursor allows for the shape control of the resultant ZnCo_2O_4 micro/nanostructures. For example, uniform and well-defined ZnCo_2O_4 microcubes with sizes of $2.0 \mu\text{m}$ (Figure 1d) can be achieved by replacing the $\text{Zn}_{0.33}\text{Co}_{0.67}\text{CO}_3$ twin microspheres with microcubes, which could originate from the different reaction pressure and dynamics of current synthetic system. The solution will be further studied in near future. Figure 1e describes the as-fabricated ZnCo_2O_4 microcubes, featuring a rough surface from the assembled secondary building blocks. From higher-magnification FESEM image of individual ZnCo_2O_4 microcube, the porous nature can be detected obviously (Figure 1e,f). The hierarchical ZnCo_2O_4 micro/nanostructures could provide both 3D networks for electron transportation and spaces critical for ion diffusion, which dominate the energy-storage performance of LIBs.

Detailed structural features about ZnCo_2O_4 hierarchical twin spheres were further characterized by transmission electron microscopy (TEM). Figure 2a indicates a low-magnification TEM image of several typical ZnCo_2O_4 twin spheres to exhibit the whole view of the 3D hierarchical twin structure with diameter of about $2.5 \mu\text{m}$, which is consistent with the observation of the FESEM images. Higher-magnification TEM image described in Figure 2b reveals that a typical ZnCo_2O_4 twin microsphere is actually a porous structure composed of many nano-sized subunits. It is also noteworthy that the primary nanosized particles uniformly distribute in the whole microspheres (Figure 2b). The HRTEM image shown in Figure 2c reveals two sets of lattice fringes with interplane spacings of 0.25 and 0.29 nm, respectively, corresponding to the (311) and (220) planes of spinel ZnCo_2O_4 phase. The crystallographic structure of the product was further identified by X-ray diffraction (XRD) as presented in Figure 2d. All the diffraction peaks can be assigned to well-crystallized cubic spinel ZnCo_2O_4 , which are in agreement with the values in the standard card (JCPDS Card No. 23–1390).

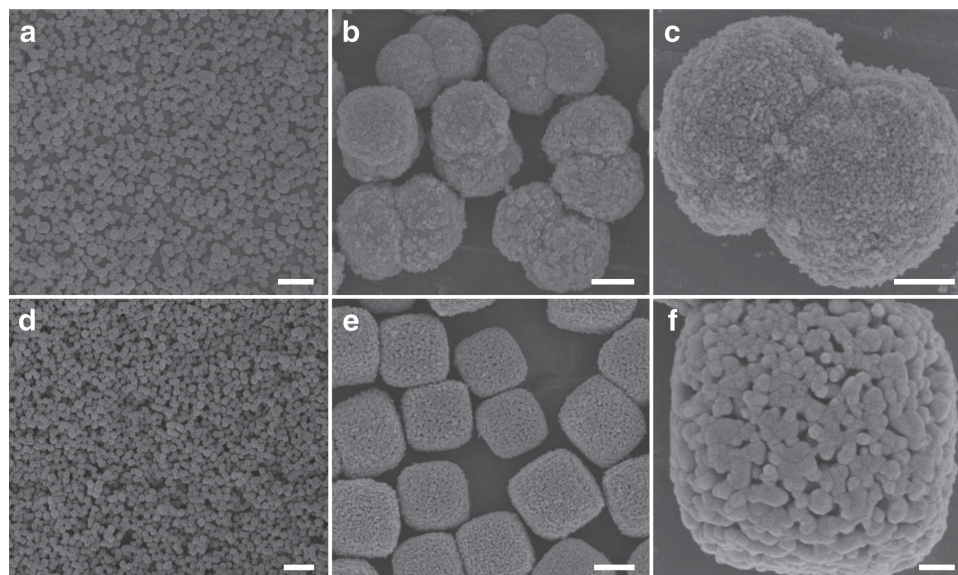


Figure 1. FESEM images of 3D hierarchical ZnCo_2O_4 (a–c) twin microspheres and (d–f) microcubes after annealing at $600\text{ }^\circ\text{C}$ for 5 h. Scale bars, $10\text{ }\mu\text{m}$ (a); $1\text{ }\mu\text{m}$ (b); $0.5\text{ }\mu\text{m}$ (c); $10\text{ }\mu\text{m}$ (d); $1\text{ }\mu\text{m}$ (e); 200 nm (f).

The schematic crystal structure of spinel ZnCo_2O_4 is demonstrated in Figure 2e. It has a normal spinel structure with the bivalent Zn-ions occupying the tetrahedral sites and the trivalent Co-ions occupying the octahedral sites in the cubic spinel structure, which are isostructural to Co_3O_4 . Energy dispersive spectroscopy (EDS) microanalysis of the ZnCo_2O_4 hierarchical twin spheres was indicated in the Supporting Information (Figure S4). The entire micro/nanostructures were found to include only Zn, Co, and O three elements, further confirming the formation of pure ZnCo_2O_4 . In order to further investigate the internal homogeneity, energy dispersive x-ray spectroscopy mapping shown in Figure 2f provides clearer information about the element distribution within the twin spheres, which unambiguously demonstrates the formation of pure ZnCo_2O_4 products.

A further investigation about the oxidation state of transition metal ions and surface analysis with X-ray photoelectron spectroscopy (XPS) for the samples studied is also presented in the supporting Information (Figure S5). The porosity trait of the ZnCo_2O_4 twin microspheres is examined by N_2 sorption at 77 K (Figure S6). The BET surface area is calculated to be about $7.33\text{ m}^2\text{ g}^{-1}$ with a relatively narrow pore size distribution ranging from $30\text{--}80\text{ nm}$. The pore volume is determined to be $0.0449\text{ cm}^3\text{ g}^{-1}$. The relatively low pore volume is mainly contributed from the small mesopores between the homogeneous nanometer-sized building blocks, which is consistent with the observation of FESEM and TEM.

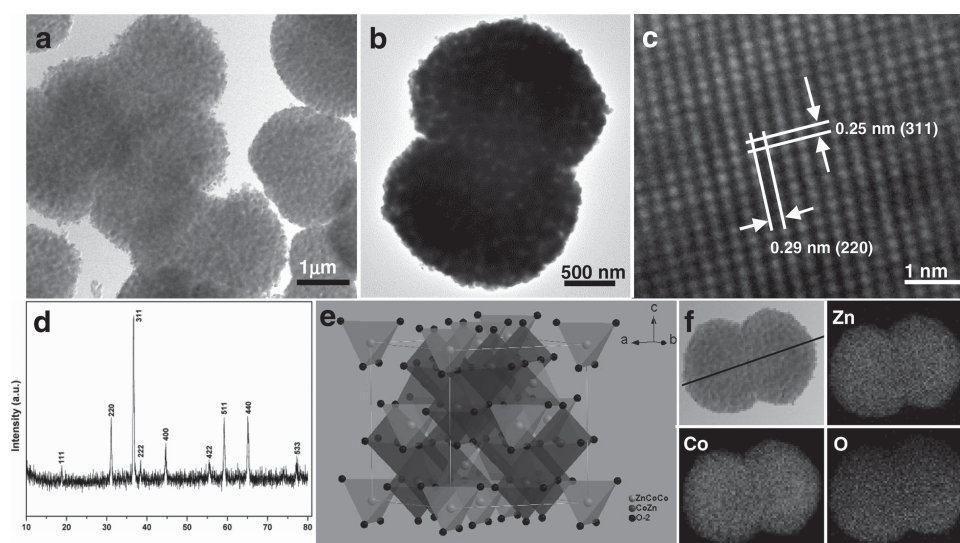


Figure 2. (a–c) TEM and high-resolution TEM images and (d) XRD pattern of hierarchical ZnCo_2O_4 twin spheres. (e) The crystal structure of spinel ZnCo_2O_4 . (f) STEM image of a single representative ZnCo_2O_4 twin sphere and the corresponding elemental mappings as well as elemental line profiles (f) of Zn, Co, and O elements.

To get more insight into the actual evolution process of 3D twin spheres of the precursor, a series of time-dependent experiments was also performed in this work, and the intermediate solids were thus sampled at the different reaction stages (nucleation and growth, etc.). **Figure 3** shows typical TEM images for the samples collected stepwise after 1.0, 1.5, 2.0, 2.5, 3.0 and 4.0 h of reaction. These sequential images reveal a morphological evolution from chain-like nanoparticle aggregates to nanorod bundles with sheaf-like structures, fan-shaped nanorod bundles, then 3D hierarchical dumbbell-like structures, the coexistence of nanorods and 3D twin spheres, and finally to 3D twin spheres with particle assembly. The crystal structure of partial intermediates intercepted at different reaction time was further investigated by XRD and IR techniques in Supporting Information. Figure S7a shows a typical XRD pattern of the 3D hierarchical dumbbell-like structure precursors. A strong diffraction peak around 10° in the XRD pattern is characteristic of metal glycolates.^[32–34] This means that metal glycolates, and not metal carbonate, formed first in the present synthetic system. The formation of ZnCo-glycolate at this moment is also supported by FT-IR analysis (see Supporting Information, Figure S7b). In Figure S7b, we observed the appearance of CH_2 - and C-O vibrational bands from ethylene glycol unit and almost disappearance of O=C=O bands from acetate group. It is noted that the pure phase of ZnCo-carbonate rather than glycolates was obtained when the reac-

tion was prolonged to 4 h (Figure S7c). As a result, our observations of the effect of time on the morphology evolution of the precursor unambiguously reveal its fast growth nature and then complex splitting behaviors, subsequently the following in situ-dissolution-recrystallization accompanied by morphology and phase change which is different from previous reports on mere crystal splitting mechanism.^[35–38] To the best of our knowledge, a new class of crystal growth process is explored for the first time. We thus propose a multistep-splitting-in situ-dissolution-recrystallization growth mechanism to understand the formation of the 3D twin spheres based on our time-dependent TEM observations and XRD analysis.

In the initial stage of the solvothermal reaction, the fast growth of precursor generates chain-like nanoparticle aggregates then to nanorods as shown in Figure 3a,b. Due to the subsequent splitting, growth can take place at the two heads of the nanorods (shown by white arrows in Figure 3b,c and Figure S8 in Supporting Information); branched nanorods and fan-shaped nanorod bundles could be produced in sequence via the continuous crystal splitting with the increase of reaction time. The splitting growth can further occur not only from the seeded nanorods continually, but also from the freshly yielded tips of the nanorods comprising the fan-shaped nanorod bundles (Figure 3d and Figure S8). It should be noted that the orientation of freshly-formed nanorods always deviates from the longitudinal axis of 1D nanorod seeds, which results in the

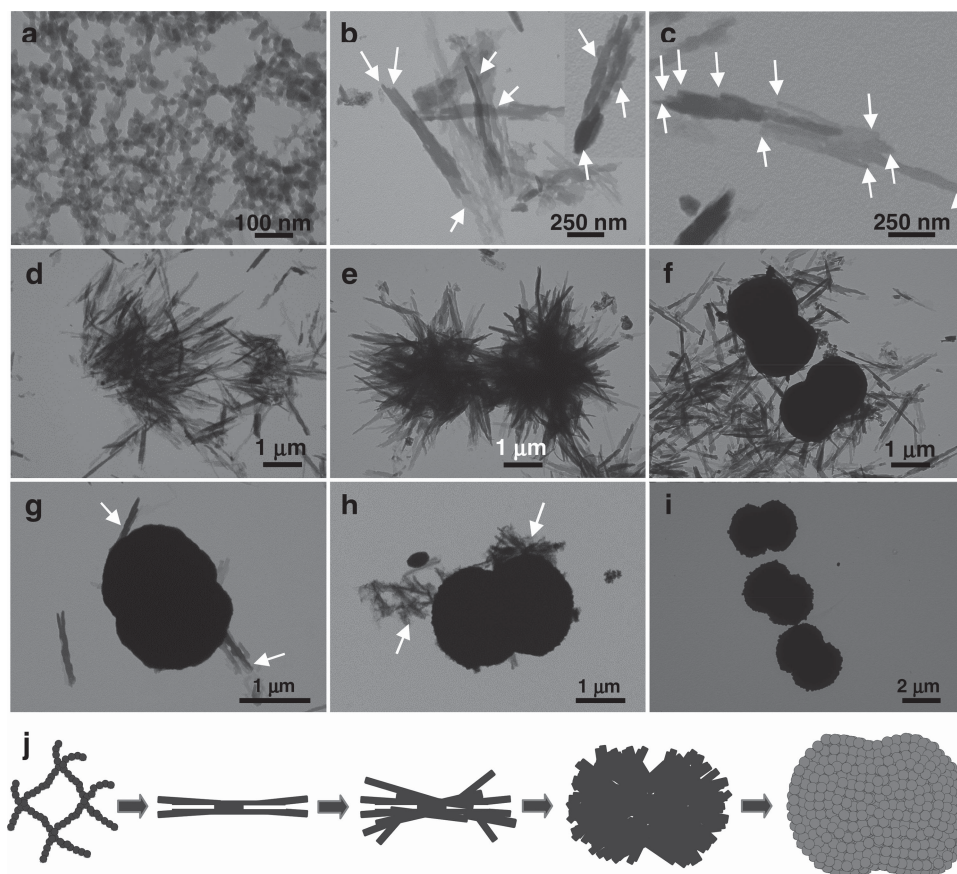


Figure 3. TEM images of the precursors synthesized at 200°C for 1 h (a); 1.5 h (b,c); 2.0 h (d,e); 2.5 h (f); 3.0 h (g,h); and 4 h (i). (j) Schematic illustration of the proposed multistep-splitting-in situ-dissolution-recrystallization growth mechanism for 3D twin spheres under the present synthetic conditions.

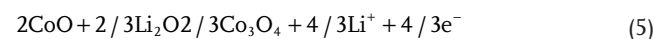
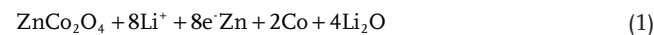
formation of 3D hierarchical twin sphere structures via the repeated and successive multistep-splitting growth (shown in Figure 3c and Figure S8). When the reaction time is more than 2.5 h, 3D hierarchical twin spheres with an unchain-like structure started to spontaneously in situ-transform to 3D hierarchical twin spheres by composed of numerous particles, which could be due to the unstability of the metastable-phase metal glycolates in our present synthetic system (Figure 3f). From Figure 3g,h and Figure S9 (see shown by white arrows), one can clearly see that the smooth surface of the nanorod bundles gradually became porous network-like nanorods composed of ultrathin sheets, and till disappeared completely, which is attached on the surface of the twin sphere. XRD patterns shown in Figure S7c clearly confirm pure hexagonal ZnCo-carbonate twin spheres by composed of primary particle were harvested via in situ-dissolution-recrystallization process when the reaction time was increased to 4 h (see Figure 3i and Figure S1a,b). The growth process of the microcubes is also investigated in detail. Very interestingly, according to the results of TEM and XRD, the formation process of the microcubes is almost similar to that of the twin microspheres (see Figure S10,11 in Supporting Information). A relatively general growth mechanism for the fabrication of novel different complex micro/nanostructures in our synthetic system has been developed.

The formation process is shown schematically in Figure 3j. The initial multistep-splitting growth can be supported by the fact that two heads of the nanorods and the fan-shaped nanorod bundles exist, as can be seen in our TEM images. Whereas the existence of some porous network-like nanorods and rod bundles may be more direct evidence for the following in situ-dissolution-recrystallization process. Our synthetic technique indeed reveals that a new crystal growth process can be achieved under the proper conditions.

The successful preparation of the 3D ZnCo₂O₄ hierarchical twin microspheres for a superior LIB anode material is evident from the extremely remarkable electrochemical behavior (as indicated in Figure 4). Figure 4a shows the first four cyclic voltammetry (CV) curves of the ZnCo₂O₄ twin microspheres electrode at a scan rate of 0.1 mV/s between 0.01 and 3.0 V. It is clearly that the curve of the first cycle in the cathodic process is substantially different from the subsequent ones. In the first cycle, the sharp peak at 0.67 V in the cathodic process can be assigned to the reduction of ZnCo₂O₄ to Zn and Co. In the anodic process, two broad oxidation peaks are observed at 1.7 and 2.2 V, usually ascribed to the oxidation of Zn to Zn²⁺ and Co to Co³⁺, respectively. In the second cycle, the cathodic peak is moved from 0.67 V to 1.1 V and becomes broader compared to the first cycle, while the anodic process almost without changes. Apparently, the differences in the second cycle indicate a different electrochemical mechanisms from the first anodic process. From the second cycle onwards, the CV curves are almost overlapped, which implies the excellent reversibility of the electrochemical reactions. The CV curves of the ZnCo₂O₄ microcubes and nanoparticles is also investigated, as shown in Figure S12. Interestingly, it was found that they showed similar electrochemical behaviors to ZnCo₂O₄ twin microspheres and there was no obvious difference in the first four consecutive CVs. That is to say, according to the results of the CVs in the only first several cycles, ZnCo₂O₄ microcubes and nanoparticles

showed the same reaction mechanism with ZnCo₂O₄ twin microspheres, it is difficult to explore the differences for their long cycling and rate performance only by CV, the main reason of the superior electrochemical performance should be owing to its unusual structural feature that can facilitate ion diffusion and accommodate the volume change during the long cycling, which will be discussed below.

Based on the above analysis, The electrochemical reactions for our mesoporous ZnCo₂O₄ electrode can be clarified as follows: [26,28]



The electrochemical performance of ZnCo₂O₄ twin microspheres have been further examined by galvanostatic discharge-charge tests at 0.5 A g⁻¹ between 0.01 and 3 V (Figure 4b). The initial discharge and charge capacities are 1288 and 954 mA h g⁻¹, respectively, corresponding to a Coulombic efficiency (CE) of 74.1%. The 25.9% capacity loss of the ZnCo₂O₄ electrode can be mainly attributed to the formation of solid electrolyte interphase (SEI) during the first charge.^[39–42] After 50 and 100 cycles, the discharge capacity are both at 1100 mA h g⁻¹, which is still higher than the theoretical value of 903 mA h g⁻¹ for ZnCo₂O₄.^[26] The extra capacities could be attributed to the synergistic effect, including the reversible formation/dissolution of polymeric gel-like film resulted from electrolyte degradation, which has also been observed in other transition metal oxides,^[43–46] and the insertion of lithium ions into interfacial storage^[45,47] and acetylene black.^[48] Generally, though the initial surface area is relatively low, however, after the first lithiation reaction, the ZnCo₂O₄ is converted to nano-grain metal particles with a diameter of 1–3 nm in the Li₂O matrix, so the surface area greatly increased. Moreover, due to the conversion character of ZnCo₂O₄, fresh metal surface is generated in every cathodic process, and so additional electrolyte decomposition is need to form SEI films, which result in slightly higher capacity than theoretical value. As our experiments are conducted using coin cell, the electrolyte to active material ratio (1mg to about 0.5 mL) is much abundant than the commercial, so the electrolyte is enough for the long cycle life. In addition, after charge and discharge at a low current, the electrolyte can penetrate into inner part of active materials. In our case, the current density of 500 mA g⁻¹ is not very high. So, to some extent, the above situation may also happen, making inner part of ZnCo₂O₄ also involved in the conversion reactions, and then also leads to the increase of capacity. On the other hand, the uniform distribution of the primary nanoparticles could also result in the high reversible conversion storage of lithium in ZnCo₂O₄.

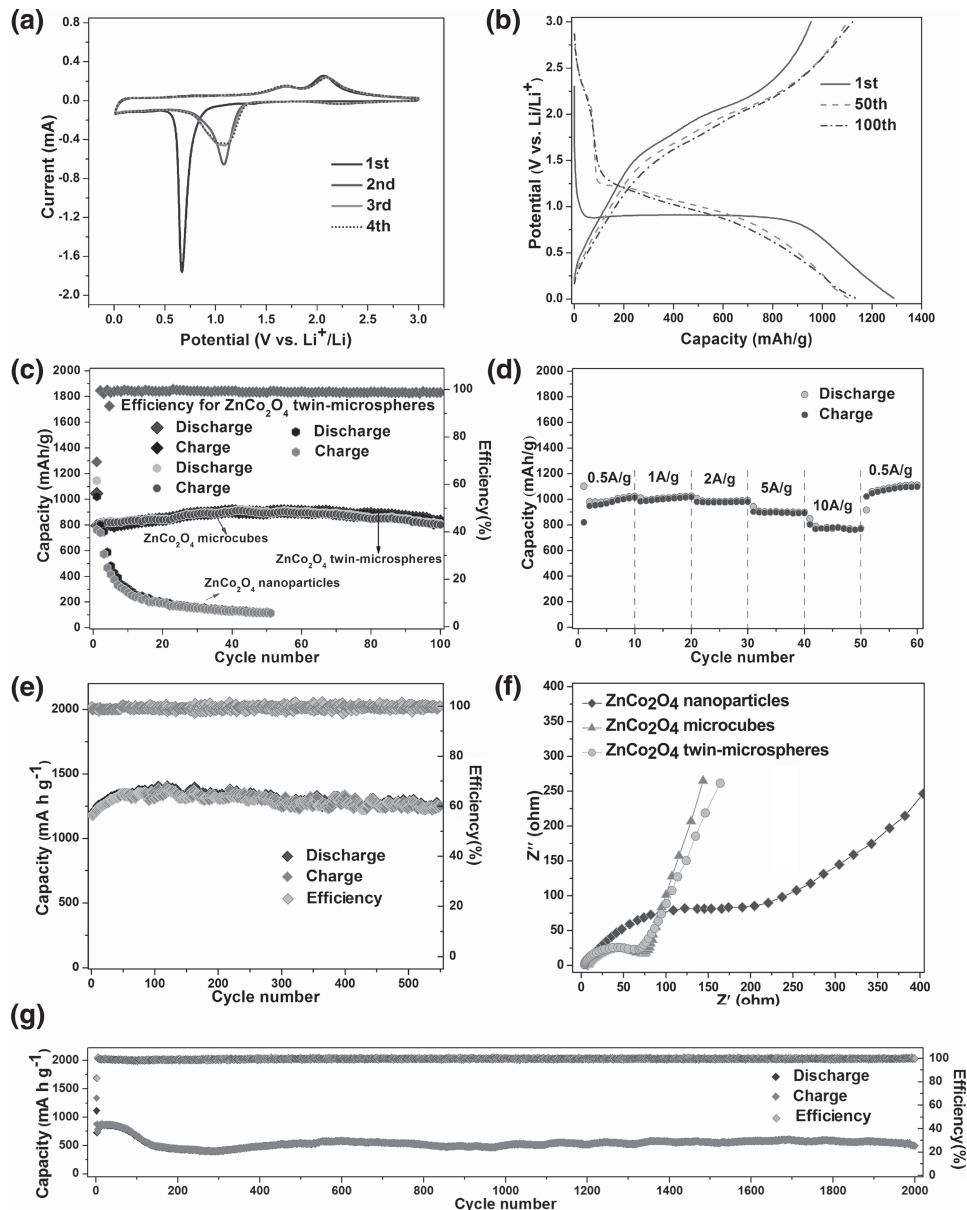


Figure 4. (a) Cyclic voltammety (CV) curves for the as-fabricated ZnCo₂O₄ twin microspheres at a scan rate of 0.1 mV s⁻¹ in the voltage window of 0.01–3.0 V. (b) Charge–discharge curves of ZnCo₂O₄ twin microspheres at a current density of 0.5 A g⁻¹. (c) Cycling performance of ZnCo₂O₄ twin microspheres, ZnCo₂O₄ microcubes and ZnCo₂O₄ nanoparticles at a current of 1 A g⁻¹. (d) Cycling performance of ZnCo₂O₄ twin microspheres at various rates. (e) The cycling performance of ZnCo₂O₄ twin microspheres after the rate test. (f) Nyquist plots of ZnCo₂O₄ twin microspheres, ZnCo₂O₄ microcubes and ZnCo₂O₄ nanoparticles at fresh cells in the frequency range from 0.1 MHz to 0.01 Hz. (g) Cycling performance of ZnCo₂O₄ twin microspheres at rates of 5 A g⁻¹.

To express the unique superiority of our mesoporous micro/nanostructures, the cycling performance of ZnCo₂O₄ twin microspheres, microcubes and nanoparticles (Figure S13, see Supporting Information) are tested at a current of 1 A g⁻¹ for 100 cycles in the voltage range of 0.01 V to 3.0 V versus Li/Li⁺ (Figure 4c). The samples of ZnCo₂O₄ twin microspheres and microcubes deliver the capacity of discharge 1145 and 1045.3 mA h g⁻¹, respectively. After 100 cycles, there are still 831.7 and 811.7 mA h g⁻¹ reserved, (about 73.1% and 77.5% retention). Furthermore, the coulombic efficiency increases to

nearly 99% after the second cycle. For comparison, ZnCo₂O₄ nanoparticles with an average diameter of about 20–30 nm in the Supporting Information (Figure S13) were also analyzed under the same conditions and the results are shown in Figure 4c. The initial capacity of discharge for ZnCo₂O₄ nanoparticles is 1022.9 mA h g⁻¹, showing no great difference from those of the above two samples. After 50 cycles, however, the capacity fades very rapidly during the first few cycles, lower capacity of 114.2 mA h g⁻¹ (only 11.1% retention) remained at the end of the 50 cycles. These data suggest that the relatively

orderly porous micro/nanostructures can provide extra space for the Li-ions and electrons insertion/extraction during cycling and hence result in excellent cycle performance and stability.

As expected, ZnCo₂O₄ twin microspheres electrode also indicates remarkable rate performance (shown in Figure 4d). Remarkably, the discharge capacity (1040 mA h g⁻¹) at 1 A g⁻¹ is even larger than that at lower current density (0.5 A g⁻¹). Similar phenomena have been reported by Zhou and Lazarraga et al.^[49,50] As the current densities increase from 1.0, 2.0, and 5.0 A g⁻¹, the electrode exhibits excellent capacity retention, slightly varying from 1040, 1005, and 920 mA h g⁻¹. When the rate was further increased to 10 A g⁻¹, the specific capacity recorded is exceptionally high at 790 mA h g⁻¹. Noticeably, when the current rate turns back to 0.5 A g⁻¹, the capacity can be retained as high as 1260 mA h g⁻¹ even after 600 cycles without any losses and the coulombic efficiency is almost around 99% (see Figure 4e). The results suggest the structure of the ZnCo₂O₄ twin microspheres maintains extraordinarily stable even under high rate long-cycling and this is very important for practical application. To further probe the high rate properties of the samples, the as-prepared ZnCo₂O₄ twin microspheres are then tested as anodes for LIBs at higher current rate of 5.0 A g⁻¹. The reversible capacity is 550 mA h g⁻¹ after 2000 cycles. Meanwhile, the coulombic efficiency is very close to 100% all over the 2000 cycles (Figure 4g). It is noteworthy that the discharge capacity gradually reduces and stabilizes at around 470 mA h g⁻¹ after about 200 cycles. Interestingly, the capacity starts to increase to high value during the subsequent 200 cycles and retains a value as high as 550 mA h g⁻¹ after 2000 cycles, which is still much higher than the theoretical capacity of graphite (372 mA h g⁻¹). Such phenomena are often observed in some transition metal oxides generally due to the reversible growth of the electro-chemistry active polymeric gel-like film by the kinetically activated electrolyte degradation.^[44,46,51–53] Not all the surface particle is covered on the initial discharge. The internal surface is more difficult to access. So the polymer layer would be constructed slowly after many cycles. Of course, the specific reasons need to be studied further. The cycling stability and rate performance of the mesoporous ZnCo₂O₄ microcubes also investigated (see Supporting Information, Figure S14 & 15). It still delivers a capacity of 478 mA h g⁻¹ at the current density of 5 A g⁻¹ after 2000 cycles, and meanwhile its rate performance is also outstanding, which further testifies extraordinary cycling stability of these 3D hierarchical micro/nanostructures even at high charge/discharge rates. To the best of our knowledge, such rate performance and cycling stability at so high charge/discharge rates are significantly higher than most documents reported about ZnCo₂O₄ micro/nanostructures and ZnCo₂O₄-based heterostructures.^[26–31]

To further clarify the superior electrochemical performance of ZnCo₂O₄ twin microspheres, the Nyquist plots are drawn (Figure 4f). Obviously, it can be seen that the diameter of the semicircle for ZnCo₂O₄ twin microspheres and ZnCo₂O₄ microcubes is similar but much smaller than that of the ZnCo₂O₄ nanoparticles at the high frequency, implying ZnCo₂O₄ twin microspheres and ZnCo₂O₄ microcubes both have lower contact and charge-transfer impedances. At the low frequency region, more vertical straight lines of our hierarchical structures compared to the ZnCo₂O₄ nanoparticles are

further evident for the faster Li⁺ ion diffusion behavior of the ZnCo₂O₄ twin microspheres and ZnCo₂O₄ microcubes. This indicates that the electron transfer and ion diffusion of our unique porous hierarchical micro/nanostructures are much faster than that of ZnCo₂O₄ nanoparticles during the charge and discharge process and thus lead to outstanding improvement on the rate performance.

The excellent electrochemical performance of our samples originates from the unique porous hierarchical architecture. On the one hand, the uniform distribution of the primary small-sized nanoparticles in the ZnCo₂O₄ hierarchical microstructure can not only provide extra active position for Li⁺ storage, but also effectively shorten the pathway for Li⁺ diffusion, which may contribute to the improved electrochemical performance towards lithium storage and better rate capability. Meanwhile, the ability of the nanoscale interspaces between nanoparticles to improve Li storage also devotes to high capacity. More importantly, the unique mesoporous architecture of the as-synthesized ZnCo₂O₄ products could significantly enhance the structural integrity by partially mitigating the mechanical strain associated with the repeated Li⁺ insertion/extraction processes during cycling demonstrated by preservation of the integrity of morphology after 30 discharge-charge cycles at 2.0 A g⁻¹ (Figure S16 in Supporting Information), which might contribute greatly to the excellent cycling stability. It is noteworthy that twin spherical hierarchical architecture possesses lower surface energy, which leads to less extent of self-aggregation during charge/discharge process. On the other hand, the intrinsic properties of zinc, such as lithium alloying reaction, also contributed to the electrochemical performance.

3. Conclusion

We have designed an effective route to synthesize two ZnCo₂O₄ micro/nanostructures via a topotactic conversion from Zn_{0.33}Co_{0.67}CO₃ twin microspheres and microcubes in laboratory air. It was found that the reaction time and the amount of ammonium bicarbonate could sensitively affect the formation of the ZnCo₂O₄ twin spheres. More significantly, a brand-new crystal growth process, a multistep-splitting-then-in situ-dissolution-recrystallization, is explored for the first time, opening up new research opportunity for investigating the formation of novel micro/nanostructures. In both structures, the ZnCo₂O₄ microstructures were composed of the primary nanocrystallites. The ZnCo₂O₄ twin spheres displayed better capacity retention, exceptionally high rate performance and ultralong cyclic stability. Taking into consideration the facile synthetic approach that prepares the unique micro/nanostructures, the ZnCo₂O₄ samples have the potential for being a high-energy and high-power anode material for LIBs. We conclude that the excellent electrochemical performance originates from the unique mesoporous hierarchical micro/nanostructures, which provide short pathway for Li⁺ and electrolyte diffusion in the pores, and meanwhile can effectively alleviate the volume change of anodes based on the conversion reaction during the repeated Li⁺ insertion/extraction. Nevertheless, the intrinsic properties of zinc, such as lithium alloying-de-alloying reaction, is also favorable for the electrochemical performance.

4. Experimental Section

Chemicals: Ethylene glycol ($\text{HOCH}_2\text{CH}_2\text{OH}$, absolute for analysis), are bought from Wuxi Zhanwang Chemical Reagent Co. Ltd in China. All the reagents, including $\text{Zn}(\text{CH}_3\text{COO})_2 \cdot 2\text{H}_2\text{O}$ (99%, AR), $\text{Co}(\text{CH}_3\text{COO})_2 \cdot 4\text{H}_2\text{O}$ (99%, AR), and NH_4HCO_3 (99%, AR), were supplied by Shanghai Sinopharm Chemical Reagent Co. Ltd. Among them, $\text{Zn}(\text{CH}_3\text{COO})_2 \cdot 2\text{H}_2\text{O}$, $\text{Co}(\text{CH}_3\text{COO})_2 \cdot 4\text{H}_2\text{O}$, NH_4HCO_3 are grounded manually for several minutes before used to accelerate the dissolution rate in the solvent and others are directly used without any treatment.

Materials Synthesis: In a typical synthesis, 0.5 mmol of $\text{Zn}(\text{CH}_3\text{COO})_2 \cdot 2\text{H}_2\text{O}$, 1 mmol of $\text{Co}(\text{CH}_3\text{COO})_2 \cdot 4\text{H}_2\text{O}$ and 15 mmol of NH_4HCO_3 were dissolved in 40 mL of $\text{HOCH}_2\text{CH}_2\text{OH}$ under stirring. After stirring for 1 h, the transparent solution was transferred into a 60 mL Teflon-lined stainless steel autoclave and maintained at 200 °C for 20 h. After the autoclave was cooled naturally to room temperature, samples depositing at the bottom were collected and washed by centrifugation for several cycles using deionized water (DI water) and absolute ethanol. The as-synthesized samples were then dried in a vacuum oven at 60 °C overnight to get the pink powders as the precursor. When NH_4HCO_3 were added to 30 mmol, the precursor of ZnCo_2O_4 microcubes were obtained. To obtain ZnCo_2O_4 twin microspheres and microcubes, the precursor was calcined to form black powers at 600 °C for 5 hours in air.

Instrumentation and Sample

Analysis: The phase of the as-synthesized samples was characterized by powder X-ray diffraction (XRD, Philips X'Pert Pro Super diffractometer, $\text{Cu K}\alpha$ radiation $\lambda = 1.54178 \text{ \AA}$). The XRD patterns were recorded from 10° to 80° at a scanning speed of 2° min^{-1} . Before the measurements, an amount of as-obtained samples were filled into a sample holder.

Investigation with high-resolution analytical transmission electron microscopy (TEM and HRTEM), and energy dispersive X-ray spectroscopy (EDX) were performed on a JEM-2100F operated at 200 kV. The specimens for TEM/HRTEM/EDX were prepared by dispersing solid samples in ethanol. The suspension was first treated by ultrasonication for three minutes in an ultrasonic water bath. The well-dispersed suspension was then dropped (1–2 drops in each sample preparation) onto a carbon-coated 200-mesh copper grids, followed by drying at room temperature before it was placed in the sample holder of the microscopes.

Morphological and structural investigations were carried out with field-emission scanning electron microscopy (FESEM, JSM-6700F, JEOL). In a typical measurement, the dried samples were mounted onto a copper stub using double-sided carbon tape.

Surface analysis for the samples was performed with X-ray photoelectron spectroscopy (XPS, VGESCA-LABMK II spectrometer, using a twin-anode Al $\text{K}\alpha$ (1486.6 eV) X-ray source). The X-ray photoelectron spectra of all of the interested elements were referenced to the C 1s peak arising from adventitious carbon (its binding energy was set at 284.6 eV). The as-prepared samples were mounted onto the double-sided adhesive tape on the sample stubs.

The nitrogen adsorption-desorption spectra of the samples were determined by nitrogen adsorption-desorption isotherm measurement at 77 K (Micromeritics Automatic Surface Area Analyzer Gemini 2360, Shimadzu).

Fourier transform infrared spectroscopy (FTIR) investigation was conducted using the KBr method with Bruker EQUINOX55. Each FTIR spectrum was collected after 32 scans at a resolution of 4 cm^{-1} from 400 to 4000 cm^{-1} . The dried samples (~1 mg) were mixed and grinded with about 0.1 g of KBr powder and prepared into sample slices for the FTIR measurement.

Thermogravimetric/differential thermal analyses (TG/DTA (TGA-2050 (TA Corp.)) were applied to characterize the obtained samples. The TGA measurements were carried out at a heating rate of 10 °C/min from 20 to 800 °C with an air flow-rate of 100 mL/min.

Electrochemical Characterization: To prepare a working electrode, active material (ZnCo_2O_4 , 70 wt%), conductive material (acetylene black 20 wt%), and polymer binder (Carboxy Methylated Cellulose, CMC, 10 wt%) were milled for 3 h, and then coated onto the surface of a copper foil. The diameter of the electrode is 12 mm, the thickness of

the coating is 200 μm and the density of the active material is about 1 mg cm^{-2} . The electrochemical measurements were carried out using 2032 coin cells with lithium foil as both the counter electrode and the reference electrode. 1 M LiPF_6 in a mixture of ethylene carbonate (EC), dimethylcarbonate (DMC) and diethyl carbonate (DEC) (1:1:1, v/v/v) was used as the electrolyte. The cell was assembled in an Ar-filled glovebox with both the moisture and the oxygen content below 1 ppm. The galvanostatic charge/discharge measurements were carried out using CT2001A LAND Cell test system. The cyclic voltammetry (CV) was tested in the voltage range of 0.01–3.0 V by an electrochemical workstation (LK2005A). The cyclic voltammetry (CV) was tested in the voltage of 0.01 to 3.0 V by an electrochemical workstation (CHI760D). Electrochemical impedance spectroscopy (EIS) was carried out on an electrochemical workstation (Materials Mates 510, Italia) in the frequency range from 0.1 Hz to 0.1 MHz.

Supporting Information

Supporting Information is available from the Wiley Online Library or from the author.

Acknowledgements

The authors gratefully acknowledge the financial support provided by the National Basic Research Program of China (the 973 Project of China, No. 2011CB935901), National Natural Science Fund of China (No. 21371108), Shandong Provincial Natural Science Foundation for Distinguished Young Scholar, the Independent Innovation Foundations of Shandong University (No.2012ZD008), the National Science Foundation of Shandong Province (No. ZR2012BM018), start-up funding for new faculty in Shandong University, and the Opening Project of CAS Key Laboratory of Materials for Energy Conversion (No. KF2014002).

Received: October 7, 2013

Revised: December 5, 2013

Published online: February 19, 2014

- [1] P. Poizot, S. Laruelle, S. Grugeron, L. Dupont, J. M. Tarascon, *Nature* **2000**, 407, 496.
- [2] C. H. Jiang, E. Hosono, H. S. Zhou, *Nano. Today* **2006**, 1, 28.
- [3] P. G. Bruce, B. Scrosati, J. M. Tarascon, *Angew. Chem. Int. Ed.* **2008**, 47, 2930.
- [4] Z. Y. Wang, L. Zhou, X. W. Lou, *Adv. Mater.* **2012**, 24, 1903.
- [5] L. Zhou, D. Y. Zhao, X. W. Lou, *Angew. Chem. Int. Ed.* **2012**, 51, 243.
- [6] G. X. Wang, H. Liu, J. Liu, S. Z. Qiao, G. Q. Max Lu, P. Munroe, H. Ahn, *Adv. Mater.* **2010**, 22, 4994.
- [7] J. Liu, T. E. Conry, X. Y. Song, M. M. Doeff, T. J. Richardson, *Energy Environ. Sci.* **2011**, 4, 885.
- [8] Y. K. Sun, S. M. Oh, H. K. Park, B. Scrosati, *Adv. Mater.* **2011**, 23, 5050.
- [9] O. K. Park, Y. Cho, S. Lee, H. Yoo, H.-K. Song, J. Cho, *Energy Environ. Sci.* **2011**, 4, 621.
- [10] F. Y. Cheng, J. Shen, B. Peng, Y. D. Pan, Z. L. Tao, J. Chen, *Nat. Chem.* **2011**, 3, 79.
- [11] J. Hemberger, P. Lunkenheimer, R. Fichtl, H.-A. Krug von Nidda, V. Tsurkan, A. Loidl, *Nature* **2005**, 434, 364.
- [12] H. Jin fan, M. Knez, R. Scholz, K. Nielsch, E. Pippel, D. Hesse, M. Zacharias, U. Göele, *Nat. Mater.* **2006**, 5, 627.
- [13] M. Matsuda, H. Ueda, A. Kikkawa, Y. Tanaka, K. Katsumata, Y. Narumi, T. Inami, Y. Ueda, S. H. Lee, *Nat. Phys.* **2007**, 3, 397.
- [14] W.-Y. Li, L.-N. Xu, J. Chen, *Adv. Funct. Mater.* **2005**, 15, 851.
- [15] X. W. Lou, D. Deng, J. Y. Lee, J. Feng, L. A. Archer, *Adv. Mater.* **2008**, 20, 258.

- [16] S. L. Xiong, C. Z. Yuan, X. G. Zhang, Y. T. Qian, *Chem. Eur. J.* **2009**, *15*, 5320.
- [17] C. C. Li, X. M. Yin, T. H. Wang, H. C. Zeng, *Chem. Mater.* **2009**, *21*, 4984.
- [18] X. Wang, X. L. Wu, Y. G. Guo, Y. T. Zhong, X. Q. Cao, Y. Ma, J. N. Yao, *Adv. Funct. Mater.* **2010**, *20*, 1680.
- [19] Y. Wang, H. J. Zhang, L. Lu, L. P. Stubbs, C. C. Wong, J. Y. Lin, *ACS Nano* **2010**, *4*, 4753.
- [20] S. L. Xiong, J. S. Chen, X. W. Lou, H. C. Zeng, *Adv. Funct. Mater.* **2012**, *22*, 861.
- [21] X. L. Xiao, X. F. Liu, H. Zhao, D. F. Chen, F. Z. Liu, J. H. Xiang, Z. B. Hu, Y. D. Li, *Adv. Mater.* **2012**, *24*, 5762.
- [22] R. Alcantara, M. Jaraba, P. Lavela, J. L. Tirado, *Chem. Mater.* **2002**, *14*, 2847.
- [23] J. F. Li, S. L. Xiong, Y. R. Liu, Z. C. Ju, Y. T. Qian, *ACS Appl. Mater. Interfaces* **2013**, *5*, 981.
- [24] L. Hu, P. Zhang, H. Zhong, X. R. Zheng, N. Yan, Q. W. Chen, *Chem. Eur. J.* **2012**, *18*, 15049.
- [25] J. F. Li, S. L. Xiong, X. W. Li, Y. T. Qian, *Nanoscale* **2013**, *5*, 2045.
- [26] Y. Sharma, N. Sharma, G. V. Subba Rao, B. V. R. Chowdari, *Adv. Funct. Mater.* **2007**, *17*, 2855.
- [27] D. Deng, J. Y. Lee, *Nanotechnology* **2011**, *22*, 355401.
- [28] N. Du, Y. F. Xu, H. Zhang, J. X. Yu, C. X. Zhai, D. R. Yang, *Inorg. Chem.* **2011**, *50*, 3320.
- [29] Y. C. Qiu, S. H. Yang, H. Deng, L. M. Jin, W. S. Li, *J. Mater. Chem.* **2010**, *20*, 4439.
- [30] L. L. Hu, B. H. Qu, C. C. Li, Y. J. Chen, L. Mein, D. N. Lei, L. B. Chen, Q. H. Li, T. H. Wang, *J. Mater. Chem. A* **2013**, *1*, 5596.
- [31] B. Liu, J. Zhang, X. F. Wang, G. Chen, D. Chen, C. W. Zhou, G. Z. Shen, *Nano Lett.* **2012**, *12*, 3005.
- [32] X. Jiang, Y. Wang, T. Herricks, Y. Xia, *J. Mater. Chem.* **2004**, *14*, 695.
- [33] Y. Wang, X. Jiang, Y. Xia, *J. Am. Chem. Soc.* **2003**, *125*, 16176.
- [34] F. Tao, C. Gao, Z. Wen, Q. Wang, J. Li, Z. Xu, *J. Solid State Chem.* **2009**, *182*, 1055.
- [35] J. Tang, A. P. Alivisatos, *Nano Lett.* **2006**, *6*, 2701.
- [36] X. F. Shen, X. P. Yan, *Angew. Chem. Int. Ed.* **2007**, *46*, 7659.
- [37] L. S. Li, N. Sun, Y. Huang, Y. Yin, N. Zhao, J. Gao, M. Li, H. Zhou, L. Qi, *Adv. Funct. Mater.* **2008**, *18*, 1194.
- [38] Y. H. Xiao, S. J. Liu, F. Li, A. Q. Zhang, J. H. Zhao, S. M. Fang, D. Z. Jia, *Adv. Funct. Mater.* **2012**, *22*, 4052.
- [39] R. Demir-Cakan, Y.-S. Hu, M. Antonietti, J. Maier, M.-M. Titirici, *Chem. Mater.* **2008**, *20*, 1227.
- [40] H. Wang, L.-F. Cui, Y. Wang, H. S. Casalongue, J. T. Robinson, Y. Liang, Y. Cui, H. Gai, *J. Am. Chem. Soc.* **2010**, *132*, 13978.
- [41] B. Z. Jang, C. Liu, D. Neff, Z. Yu, M. C. Wang, W. Xiong, A. Zhamu, *Nano Lett.* **2011**, *11*, 3785.
- [42] S. W. Lee, N. Yabuuchi, B. M. Gallant, S. Chem, B.-S. Kim, P. T. Hammond, Y. Shao-Horn, *Nat. Nanotechnol.* **2010**, *5*, 531.
- [43] S. Laruelle, S. Grugeon, P. Poizot, M. Dolle, L. Dupont, J. M. Tarascon, *J. Electrochem. Soc.* **2002**, *149*, A627.
- [44] G. M. Zhou, D. W. Wang, F. Li, L. L. Zhang, N. Li, Z. S. Wu, L. Wen, G. Q. Lu, H. M. Cheng, *Chem. Mater.* **2010**, *22*, 5306.
- [45] S. Grugeon, S. Laruelle, L. Dupont, J. M. Tarascon, *Solid State Sci.* **2003**, *5*, 895.
- [46] J. S. Do, C. H. Weng, *J. Power Sources* **2005**, *146*, 482.
- [47] P. Balaya, H. Li, L. Kienle, J. Maier, *Adv. Funct. Mater.* **2003**, *13*, 621.
- [48] Y. Deng, Q. Zhang, S. Tang, L. Zhang, S. Deng, Z. Shi, G. Chen, *Chem. Commun.* **2011**, *47*, 6828.
- [49] L. Zhou, D. Y. Zhao, X. W. Lou, *Angew. Chem. Int. Ed.* **2012**, *51*, 239.
- [50] M. G. Lazarraga, L. Pascual, H. Gadjev, D. Kovacheva, K. Petrov, J. M. Amarilla, R. M. Rojas, M. A. Martin-Luengo, J. M. Rojo, *J. Mater. Chem.* **2004**, *14*, 1640.
- [51] S. Grugeon, S. Laruelle, L. Dupont, J. M. Tarascon, *Solid State Sci.* **2003**, *5*, 895.
- [52] F. M. Courtel, H. Duncan, Y. Abu-Lebdeh, I. J. Davidson, *J. Mater. Chem.* **2011**, *21*, 10206.
- [53] G. Q. Zhang, L. Yu, H. B. Wu, H. E. Hoster, X. W. Lou, *Adv. Mater.* **2012**, *24*, 4609.